Ceramics International 50 (2024) 16998–17010

Contents lists available at ScienceDirect

Ceramics International

journal homepage: www.elsevier.com/locate/ceramint

Fabrication of novel strontium-coated bioactive ceramic-glass ($C_2S(2P_6)C_2S$) 3D-porous scaffold for the proliferation and osteogenic differentiation of bone marrow-derived mesenchymal stem cells

Jeevithan Elango [a,b,c], Karina Salazar [d], Pablo Velasquez [d], Angel Murciano [e], Piedad N. de Aza [d,*], Wenhui Wu [c], José Manuel Granero Marín [f], Jose E. Mate Sanchez de Val [a,**]

[a] Department of Biomaterials Engineering, Faculty of Health Sciences, UCAM-Universidad Católica San Antonio de Murcia, Campus de los Jerónimos 135, Guadalupe, 30107, Murcia, Spain
[b] Center of Molecular Medicine and Diagnostics (COMManD), Department of Biochemistry, Saveetha Dental College and Hospitals, Saveetha Institute of Medical and Technical Sciences, Saveetha University, Chennai, 600077, India
[c] Department of Marine Biopharmacology, College of Food Science and Technology, Shanghai Ocean University, Shanghai, 201306, China
[d] Instituto de Bioingeniería, Universidad Miguel Hernández, Avda. Ferrocarril s/n, Elche, Alicante, 03202, Spain
[e] Departamento de Materiales, Óptica y Tecnología Electrónica, Universidad Miguel Hernández, Avda. Universidad s/n, Elche, Alicante, 03202, Spain
[f] Department of Restorative Dentistry, Faculty of Medicine and Dentistry, UCAM-Universidad Católica San Antonio de Murcia, Campus de los Jerónimos 135, Guadalupe, 30107, Murcia, Spain

ARTICLE INFO

Handling editor: Dr P. Vincenzini

Keywords:
Bioceramics
Strontium-ceramic-glass composite 3D scaffolds
Mesenchymal stem cells
Osteogenic differentiation

ABSTRACT

This study fabricated novel multilayer 3D-scaffolds by coating bioactive Calcium silicate (Ca_2SiO_4)/glass phase (calcium ultraphosphate, $Ca_2P_6O_{17}$)/Ca_2SiO_4 ($C_2S(2P_6)C_2S$) 3D scaffolds with strontium (Sr) for osteogenic differentiation of bone marrow-derived mesenchymal stem cells (MSCs). Hence, for the first time, $C_2S(2P_6)C_2S$/Sr 3D-scaffolds were fabricated by sol-gel method and their characterization (X-Ray diffraction analysis (XRD), scanning electron microscopy (SEM) and Mercury Porosimetry), effect in MSCs proliferation (cytotoxicity and mRNA expression) and osteogenic differentiation (staining and mRNA expression) were evaluated. The porosity and SEM data showed that the porosity (31.66% for $C_2S(2P_6)C_2S$ and 32.14% for $C_2S(2P_6)C_2S$/Sr), pore size (<300 μm) and microstructure were not altered between $C_2S(2P_6)C_2S$ and $C_2S(2P_6)C_2S$/Sr 3D-scaffolds, respectively. MSCs proliferation rate was increased by $C_2S(2P_6)C_2S$/Sr 3D-scaffold via upregulating c-Fos and TGF-β1 mRNA expression. Alizarin Red (calcium), von-kossa (calcium-phosphate) and alkaline phosphatase (ALP) staining were higher in differentiated MSCs cultured on $C_2S(2P_6)C_2S$/Sr 3D scaffold than in control. The osteogenic stimulatory effect of $C_2S(2P_6)C_2S$/Sr 3D scaffold could be justified by increasing osteogenic stimulatory genes such as collagen type-I, Runx2, osteocalcin and ALP expression in differentiated MSCs. Further, SEM images proved that the C2S(2P6)C2S/Sr 3D scaffold-cultured cells had unique morphology similar to biological tissues. Accordingly, this is the first report evidencing the MSC proliferative and osteogenic stimulatory ability of strontium-coated $C_2S(2P_6)C_2S$ 3D-scaffold, which greatly impacts future strategic therapies in dentistry and bone regeneration.

1. Introduction

Modern regenerative therapies always require new approaches for fabricating innovative biomaterials in order to compromise the mechanical and biological behaviour in practical applications [1–3]. In this sense, several biomaterials derived from natural and synthetic materials are investigated in recent times with surface modification to manipulate the functional properties of implants [4–6]. Among the

* Corresponding author.
** Corresponding author.
E-mail addresses: srijeevithan@gmail.com, jelango@ucam.edu (J. Elango), karina.salazar@goumh.umh.es (K. Salazar), pavelasquez@umh.es (P. Velasquez), amurciano@umh.es (A. Murciano), piedad@umh.es (P.N. de Aza), whwu@shou.edu.cn (W. Wu), jemate@ucam.edu (J.E. Mate Sanchez de Val).

https://doi.org/10.1016/j.ceramint.2024.02.175
Received 20 September 2023; Received in revised form 21 January 2024; Accepted 14 February 2024
Available online 15 February 2024

Table 1
Compositions (mol%) of the ceramic/glass/ceramic 3D scaffolds.

Sample	Ceramic		Glass			Ceramic		
	TEOS	$CaCO_3$	TEP	$CaCO_3$	Li_2CO3	TEOS	$CaCO_3$	$SrCO_3$
C_2S	33.33	66.66	–	–	–	–	–	–
$C_2S(2P_6)$	33.33	66.66	71.73	23.91	4.34	–	–	–
$C_2S(2P_6)C_2S$	33.33	66.66	71.73	23.91	4.34	33.33	66.66	–
$C_2S(2P_6)C_2S$–Sr	33.33	66.66	71.73	23.91	4.34	33.35	65.99	0.67

different bioactive implants, bioactive ceramic is a widely studied material in different applications including bone, dental, orthopedic and skin regeneration [7–10]. The major limitation of bioactive ceramic is inadequate bioactivity and the release of unfavorable ions from the surface of the implant, which could develop adverse effects by inhibiting the direct contact between surrounding tissue and substrate [11,12].

Dicalcium silicate (C_2S), a bioactive ceramic, has been widely investigated due to its excellent bioactivity, biodegradability and biocompatibility [13–15]. For instance, different types of hybrid C_2S-based bioceramics have been fabricated for osteogenic and angiogenic responses [16–19], odontogenic and angiogenic differentiation of human periodontal ligament cells [20] and bone regeneration [13]. Though, C_2S-based materials are widely used in several applications, the deleterious biological effects due to their high dissolution rate and pH induction within the surrounding tissues limit their biomedical applications [13,21–23]. In addition to C2S, another bioceramic, calcium pyrophosphate (Ca2P2O7) is a well-known inhibitor for HA crystal formation,and thus potentially control the biomineralization process [24]. However, the above downregulating effect in biomineralization process is inhibited via hydrolyzing pyrophosphate ions by the alkaline phosphatase (ALP) secreted from active osteoblasts, which simultaneously switch-on HA formation and supersaturates the extra-cellular fluid with orthophosphates to induce mineralization [24–26]. This mechanism is critical to control the homeostasis of biomineralization in bones. Pyrophosphates are relatively unexplored in bone graft replacement applications, despite decades of research demonstrating the role of this ion in bone [27,28].

In order to obtain suitable materials that meet the standards for bone tissue applications,a multilayer design with different functions of each layer is proposed [29–32]. For instance, the internal layer should mechanically improve the material for better control of biodegradability and bioactivity. At the same time, the external layer, in contact with the tissue, should improve the cell adhesion, receptor interaction, signaling pathways and biological functions of biomaterials employed in clinical applications. In this sense, the external layer could be coated with ions such as strontium (Sr), which is a trace element in the human body andplays a major role in stimulating bone formation and inhibiting bone resorption [33,34]. It has been evidenced that Sr treatment could increase the bone strength, and inhibit the incidences of fractures in osteoporosis [35] due to its antiresorptive and anabolic activity, respectively. Earlier research claimed that coating of Sr in calcium phosphate cement improved the compressive strength, radiopacity, setting time, cell adhesion, proliferation and osteogenic differentiation of human mesenchymal stem cells (MSCs) and thereby enhanced the new bone formation at the bone−materials interface [34]. In general, the use of bone marrow derived MSCs have been recognized as a gold standard method to investigate the osteogenic potential of several biomaterials [2,4,5,17], hence the present study used bone marrow-derived MSCs to investigate the osteogenic potential of Calcium silicate (Ca_2SiO_4)/glass phase (calcium ultraphosphate, $Ca_2P_6O_{17}$)/Ca_2SiO_4 ($C_2S(2P_6)C_2S$) 3D scaffolds.

Based on the above discussion, a multilayer material designed for the specific requirements of the different implantation sites is an unavoidable concept for the current stratergies in clinical treatment. Hence, the present study hypothesized that the fabrication of multilayer ceramic/glass/ceramic ($C_2S(2P_6)C_2S$) 3D scaffolds with an active functional surface coating of Sr due to their bone stimulatory effect could be an appropriate approach in the development of bioceramics for bone and dental tissue engineering. However, none of the studies investigated the biocompatibility and osteogenic differentiation ability of Sr-coated $C_2S(2P_6)C_2S$ 3D-scaffolds using bone marrow MSCs. Therefore for the first time, the present study aimed to fabricate Sr-coated $C_2S(2P6)C_2S$ 3D scaffolds and investigated the influence of Sr coating on scaffold's characterization, biocompatibility and osteogenic differentiation of bone marrow-derived MSCs.

2. Materials and methods

2.1. Fabrication of ceramic/glass/ceramic scaffolds with and without strontium

The 3D porous ceramic/glass/ceramic scaffolds were prepared by the sol-gel method together with the polymeric replica technique using20 ppi DINA4 10 mm sponges (Quality Materials, Barcelona, Spain). The fabrication process of 3D scaffold was consisted three different stages as mentioned below.

2.1.1. Synthesis of the dicalcium silicate (C_2S) core

In the first stage, the dicalcium silicate (Ca_2SiO_4) core was obtained from the commercial chemicals: TEOS (Tetraethyl orthosilicate, Aldrich ≥98%) and $CaCO_3$ (Calcium carbonate, Sigma ≥99%). The hydrolysis of the precursor was carried out using hydrochloric acid, obtaining a homogeneous mixture with a pH in the range of 2–3. Once the solution was obtained, the polymeric sponge (13 mm∅, 10 mm long) was submerged 30–40 times, and dried at 160–180 °C for 15 min after each immersion. Then, a heat treatment was applied, consisting of heating up to 1050 °C for8h.

2.1.2. Fabrication of $C_2S(2P_6)$ scaffolds

In the second stage, the core was coated with a glass phase ($Ca_2P_6O_{17}$) from the reagents TEP (Aldrich triethyl phosphate ≥99.8%), $CaCO_3$ (calcium carbonate, Sigma ≥99%) and Li_2CO_3 (Lithium carbonate, Sigma-Aldrich 99.8 ≥%). The hydrolysis of the reagents was carried out using hydrochloric acid, keeping the mixture at a 4–5 pH. In this case, the previously prepared C_2S core was immersed 10 times in the new solution described, and dried at 140–160 °C for 10 min after each immersion. After this step, a heat treatment was carried out at 1050 °C for 8h. To improve the mechanical resistance, this vitrification process was carried out twice (2P6).

2.1.3. Fabrication with and without strontium in $C_2S(2P_6)C_2S$ 3D scaffolds

Finally, the surface of the ceramic/glass scaffolds was modified using an external layer of C_2S ceramic coated with 1% Sr^{+2} to enhance cell adhesion behavior. The coating was prepared with TEOS, $CaCO_3$ and $SrCO_3$ (Strontium carbonate Alfa Aesar 99%). Ten coatings were made after drying at 160–180 °C for 20 min, followed by final heating at 1050 °C for 8 h. Table 1 shows the composition and label of the ceramic/glass/ceramic 3D scaffolds. Finally, two kinds of multilayer scaffolds were fabricated such as $C_2S(2P6)C_2S$ 3D scaffolds and Sr-coated $C_2S(2P6)C_2S$ 3D scaffolds for the following experiments.

2.2. Characterization of the ceramic/glass/ceramic 3D scaffolds

The characterization of the crystalline phases present in the 3D scaffolds was carried out by X-ray Diffraction (XRD) (DRX Bruker-AXR D8Advance), in the 2 theta 10–55 range, using Cu-Kα radiation. (1.5418740 Å). The X-ray tube was operated at 40 kV and 30 mA (Match Software Version 3.7.1.132). The diffractograms of samples (n = 3) were compared with the Crystallography Open Database (COD) and the Inorganic Crystal Structure Database (ICSD). All diffractograms were analyzed by version 3.7.1.132 of the Match software. The surface morphology of scaffolds was captured by using Scanning electron microscopy (SEM-Hitachi S-3500 N). The porosity and pore distribution of the 3D scaffolds (n = 3) were evaluated by the Mercury Porosimetry Technique (Poremaster 60 GT Quantachrome instruments) at a pressure range between 69.38 bar and 2427560,78 bar. The higher porosity of 3D scaffolds was 300 μm determined by Archimedes' method.

2.3. Biocompatibility of the ceramic/glass/ceramic 3D scaffolds

The bone marrow-derived MSCs were cultured on 3D scaffolds to investigate the biocompatibility. The MSCs were purchased from LGC Standards, Barcelona, Spain (ATCC PCS-500-012, LGC Standards, Barcelona, Spain, Order Ref. No. 86605340) and cultured in mesenchymal stem cell medium (PCS-500-030) with growth supplements (15 ng/mL rh IGF-1, 125 pg/mL Rh FGF-b, 2.4 mM L-Alanyl-L-Glutamine (PCS-500-041), 5% fetal bovine serum (FBS) (Gibco, Waltham, MA, USA), and 1% antibiotic. The cells from passages 3 to 6 were used for the whole experiments. For the biocompatibility assessment, the cells with a density of 1×10^4 were seeded in 48 well-culture plates along with 3D scaffolds (n = 3) and cultured for 3 and 7 days with media change every two days once. All the 3D scaffolds were UV-sterilized for 30 min before cell culture. The MSCs cultured in a 2D culture plate without 3D scaffolds served as control. The proliferation rate of MSCs was estimated by MTT assay after treating cells with 5 mg/mL MTT reagent in PBS for 4 h in a CO_2 incubator with a relative humidity of 95% and 5% CO_2. After incubation, the unbound MTT reagent was removed by PBS wash and the formazan crystals were solubilized in DMSO. The dye intensity was measured by using a SpectraMax iD3 Multi-Mode MicroplateReader at 570 nm.

2.4. Cell seeding density

To investigate the total MSCs seeding capacity of 3D scaffolds, the cell seeding density method was employed by following our previous protocol [36]. In brief, the cells with a density of 1×10^5 were carefully loaded on top of the 3D scaffolds. Prior to cell seeding, the 3D scaffolds were incubated in the culture medium for 2 h. The seeded cells were allowed to attach the 3D scaffolds (n = 3) for 5 h, and then the cells seeded 3D scaffolds were re-located into new wells in order to quantify specifically 3D scaffold-bound cells. The 3D scaffold-bound cells were harvested by trypsinization using 0.25 % trypsin-EDTA solution following the standard cell-culture method. The cells cultured in 2D culture plates (n = 3) without 3D scaffolds served as control and were treated the same way as described earlier. The cell number was counted based on our previous method [36] by using an automated cell counter (Invitrogen, Countess 3 FL, Thermo Fisher Scientific, Waltham, MA, USA). The percentage of cell seeding density was calculated from the number of bound cells in each group compared to the initial loaded cell's quantity.

2.5. Osteogenic differentiation

In order to investigate the osteogenic potential of 3D scaffolds, the MSCs were differentiated into osteogenic cells with or without osteogenic supplementation. In brief, MSCs seeded with 3D scaffolds (n = 3) were cultured in osteogenic culture medium and supplements (Gibco, Reference: A10066-01, Lot No: 2419081) for 21 days. In parallel, MSCs seeded with 3D scaffolds (n = 3) were also cultured in mesenchymal stem cell culture medium without any osteogenic supplement. The cells without 3D scaffolds were considered as control.

2.6. Alkaline phosphatase (ALP) stain

The hallmark pre-osteogenic marker, ALP is widely used to confirm the osteogenic ability of biomaterials used in bone tissue engineering. Therefore, in this study, the level of ALP in cells cultured with or without 3D scaffolds and/or osteogenic culture medium was determined as per our previous method [36]. The MSCs were seeded on 3D scaffolds (n = 3) and 2D culture plates (control) (n = 3) with a cell density of 5×10^5 and cultured with or without osteogenic culture medium for 21 days. The culture medium was replaced every two to three days once for 21 days. At the end of the experiment, the cells were fixed with standard histological fixatives such as 2.5% glutaraldehyde and 4% paraformaldehyde for 30 min each. After a quick PBS wash, the cells were stained with a commercial ALP kit (Cat No. SCR004, Sigma-Aldrich, Madrid, Spain) by following the manufacturer's standard instructions.

2.7. Mineral staining

To evaluate the osteogenic potential of 3D scaffolds, the level of mineral deposition in differentiated MSCs was measured by Alizarin Red and von Kossa staining methods [36]. In brief, the MSCs with a cell density of 2×10^4 were cultured on 3D scaffolds (n = 3) for 21 days with medium change twice a week. At the end of the experiment, the cultured medium was removed, washed with PBS twice and fixed with histological fixatives (2.5% glutaraldehyde and 4% paraformaldehyde for 30 min each). The amounts of calcium and calcium phosphate mineral depositions in differentiated cells were stained with 3% alizarin red stain (Red stain) and von Kossa stain (black/brown stain) (LabClinics, Barcelona, Spain) for 30 min under dark conditions, respectively. The excess unbound stains were washed out with PBS. The images were captured in bride-field mode using fluorescence-microscopy coupled with ZEISS Axiocam 305 mono (Axio Vert A1, Serial No. 3847016567, Carl Zeiss Microscopy GmbH, Suzhou, China).

2.8. Fluorescence staining

The fluorescence staining method investigated the interaction of MSCs on 3D scaffolds. In brief, the MSCs were seeded on top of the 3D scaffolds (n = 3) and cultured for 7 days with culture medium as described earlier. The cell cytoskeleton and nuclei were visualized by FTIC and DAPI fluoroprobes. After culture, the cells were fixed with histological fixatives (2.5% glutaraldehyde and 4% paraformaldehyde) and the cell membrane was permeabilized with 0.2% Triton X-100 in PBS for 5 min at room temperature. Then, the cells were stained by FITC and DAPI fluoroprobes with PBS wash in between each step. The fluorescence images were captured by using fluorescence-microscopy coupled with ZEISS Axiocam 305 mono (Axio Vert A1, Serial No. 3847016567, Carl Zeiss Microscopy GmbH, Suzhou, China).

2.9. mRNA expression

The proliferative and osteogenic stimulatory abilities of 3D scaffolds were further evidenced by mRNA expression using quantitative real-time (qRT)-PCR method. The MSCs with a cell density of 1×10^5 for proliferation and 1×10^6 for osteogenic differentiation were seeded with 3D scaffolds (n = 3) in 12-well and 6-well-culture plates, respectively. The cells were cultured with mesenchymal stem cell culture medium for proliferation (for 7 days) and osteogenic stimulation culture medium for osteogenesis (for 21 days) as described earlier. After treatment, the total cellular RNA was extracted from the cultured cells using TRIzol reagent (Invitrogen, Waltham, MA, USA) and reverse transcribed

Table 2
List of primers used in this study.

No	Genes name	Forward	Reverse
Proliferation genes			
1	c-Fos (XM085152)	5′-GCTTTGCAGACCGAGATTGC-3′	5′-TTGAGGAGAGGCAGGGTGAA-3′
2	SMAD3	5′-CATCGAGCCCCAGAGCAATA-3′	5′-GTGGTTCATCTGGTGGTCACT-3′
3	TGF-β1	5′-GGACACCAACTATTGCTTCAGCTCC-3′	5′-AGGCTCCAAATGTAGGGGCAGGGCC-3′
Osteogenic genes			
4	Collagen type I	5′-GCG AAG GCA ACA GTC GCT -3′	5′-CTT GGT GGT TTT GTA TTC GAT GAC 3′
5	Runt-related transcription factor 2	5′-CCA CCA CTC ACT ACC ACA CG 3′	5′-TCA GCG TCA ACA CCA TCA TT 3′
6	ALP	5′-TCC TGA CCA AAA ACC TCA AAG G 3′	5′-TGC TTC ATG CAG AGC CTG C 3′
7	Osteocalcin	5′-CTC ACA GAT GCC AAG CCC 3′	5′-CCA AGG TAG CGC CGG AGT CT 3′
8	hGAPDH	5′-AGC TTG TCA TCA ACG GGA AG 3′	5′-TTT GAT GTT AGT GGG GTC TCG 3′

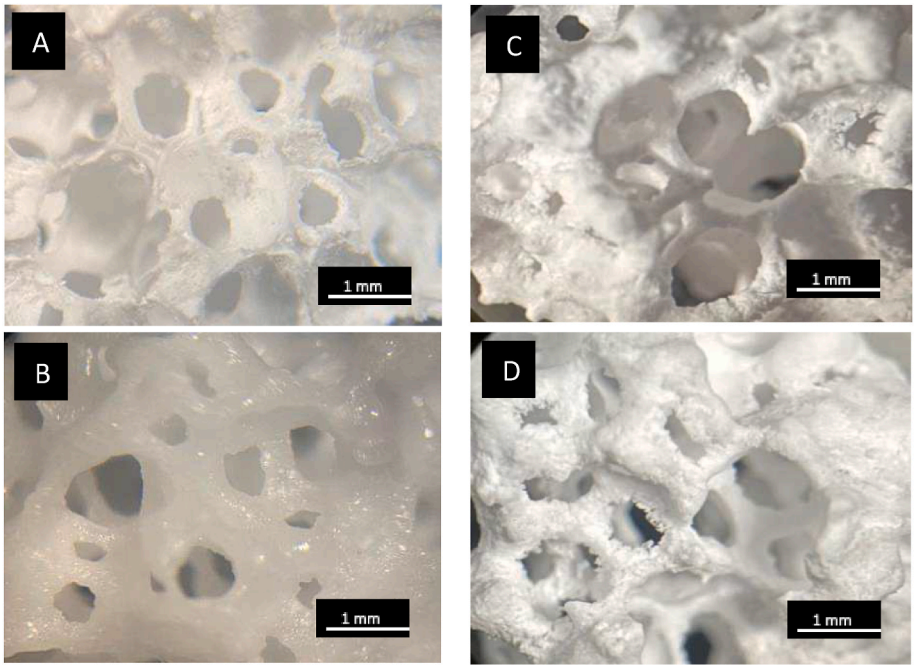

Fig. 1. Optical images of ceramic/glass/ceramic 3D scaffolds. A: C_2S, B: $C_2S(2P_6)$, C: $C_2S(2P_6)C_2S$ and D: $C_2S(2P_6)C_2S$–Sr obtained by the sol gel method.

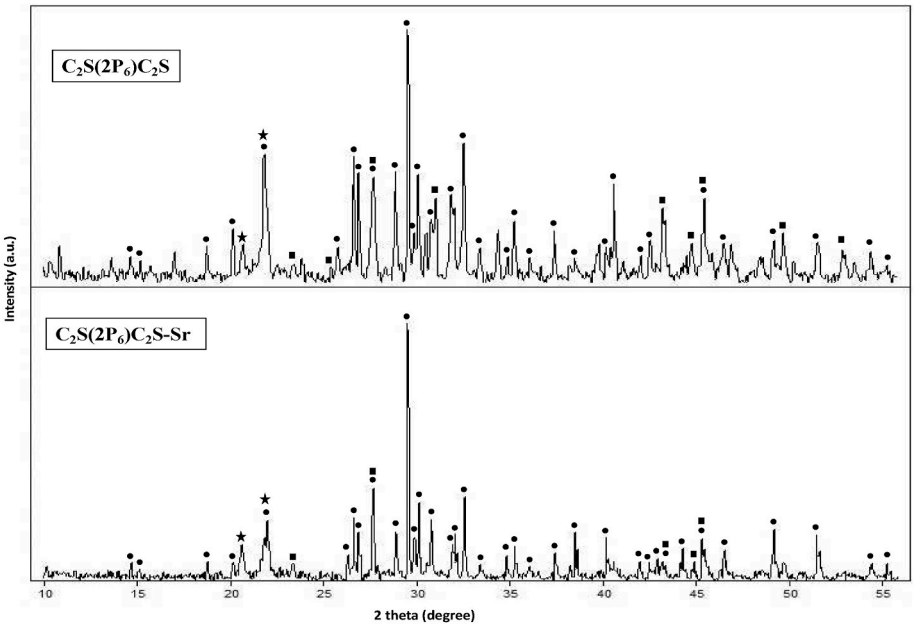

Fig. 2. XRD patterns of the ceramic/glass/ceramic 3D scaffolds (● $Ca_2P_2O_7$, ⋆ SiO_2, ∎ $CaSiO_4$).

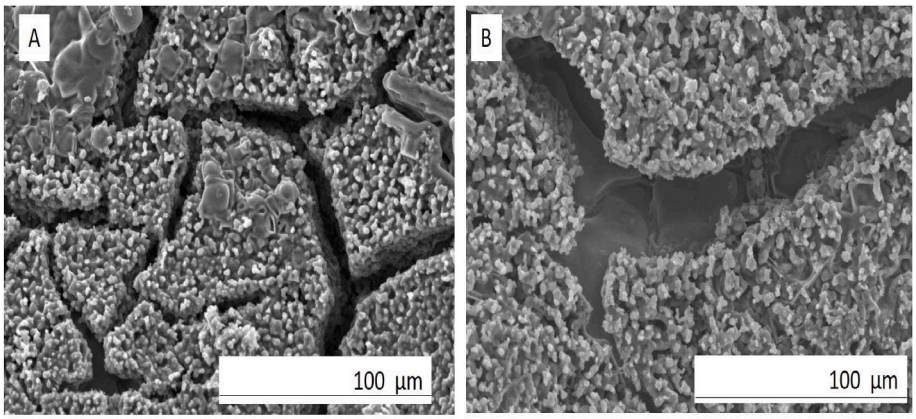

Fig. 3. SEM images of the ceramic/glass/ceramic 3D scaffolds.: (A) $C_2S(2P_6)C_2S$; (B) $C_2S(2P_6)C_2S$/Sr.

to single-strand cDNA using a cDNA first-strand synthesis kit after DNAse treatment. The PCR reaction mixture was prepared with SYBR Green Premix Ex Taq. The target proliferative (c-Fos, SMAD3 and TGF-β1) and osteogenic (Collagen type I, Runt-related transcription factor 2, osteocalcin and ALP) gene sequences were amplified in a thermocycler, an ABI 7500 real-time PCR Detection System (Applied Biosystems, Shanghai, China). The target gene expression was normalized with the housekeeping gene expression (hGAPDH). The primers (Table 2) were designed based on our previous methods [37,38].

2.10. Microstructural analysis

The microstructural features of MSCs cultured on different materials such as culture plate (control), $C_2S(2P_6)C_2S$ and $C_2S(2P_6)C_2S$/Sr 3D scaffolds were analyzed by scanning electron microscopy (SEM-Hitachi S-3500 N). Briefly, the cells were cultured as described earlier for 3 days and 7 days for proliferation and 21 days in case of osteogenic differentiation (n = 3). Then, the cells cultured on scaffolds were washed gently with PBS and fixed with fixatives (2.5 % glutaraldehyde), followed by a critical point drying method using hexamethyldisilazane (HMDS). Then, the specimens were mounted on aluminium stubs for platinum sputter-coating with 5.0 nm thin layer (Leica EM ACE 600) and captured using a FE-SEM (ApreoS Lovac IML Thermofisher, US) with a selected voltage of 10 kV and 0.20 nA at different magnifications.

2.11. Statistics

The results of the present study were collected from at least three independent experiments and were expressed as means ± SD unless otherwise indicated. The statistical difference and comparisons were made using one-way ANOVA analysis and a p-value less than 0.05 was noted as statistical significance after treating the data in GraphPad Prism 9.4.0 software.

3. Results

The different layers of the ceramic/glass/ceramic 3D scaffold structure are shown in Fig. 1. Fig. 1A and B showed the ceramic core, followed by a glass layer, representing the characteristic brightness of vitreous materials and finishing with a C_2S ceramic layer (Fig. 1C). The final scaffold showed a multilayer microstructure constituted with three layers. Fig. 1D shows the outer layer after coating with strontium. In general, no significant differences were observed between the two 3D scaffolds (Fig. 1C and D).

Fig. 2 shows the XRD diffraction patterns of the $C_2S(2P_6)C_2S$ and the $C_2S(2P_6)C_2S$/Sr 3D scaffolds. In general, the XRD of the $C_2S(2P_6)C_2S$ and the $C_2S(2P_6)C_2S$–Sr 3D scaffold showed three main phases: calcium diphosphate ($Ca_2P_2O_7$) (COD 96-100-1557), tridymite (SiO_2), (COD 96-900-0521) and calcium silicate $CaSiO_4$ (COD 96-900-8152). However, the strontium phase was not detected in XRD peak due to lower limit or the vitreous phase.

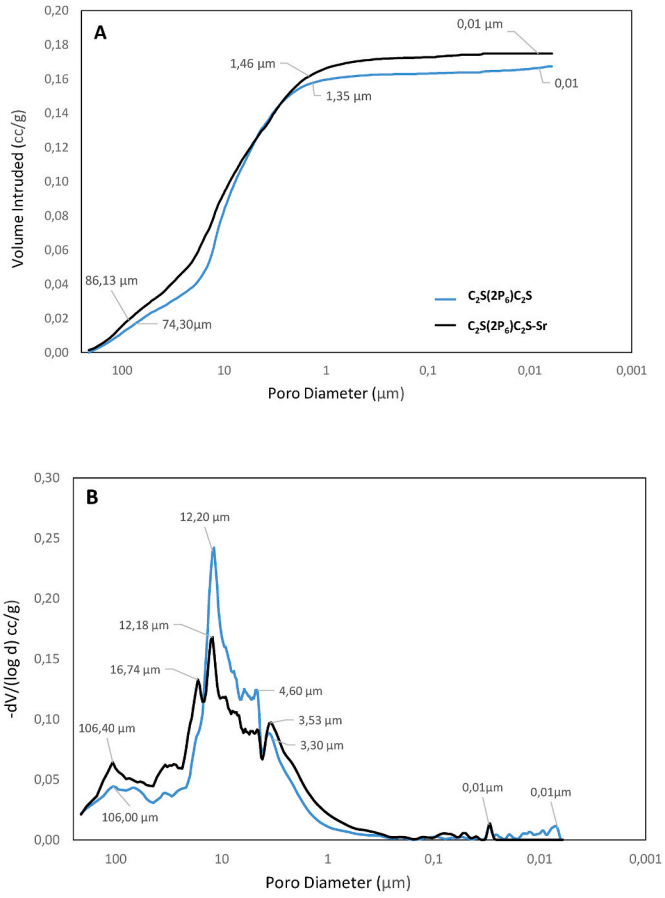

Fig. 4. Mercury porosimetry curves: (A) Cumulative and (B) Differential intrusion vs. pore diameter in ceramic/glass/ceramic 3D scaffolds.

The SEM images of the ceramic/glass/ceramic 3D scaffolds showed no significant changes in the microstructure upon coating with strontium (Fig. 3). In general, the 3D scaffolds showed a polyhedral grain structure with cracks, which might be due to the heat treatment.

The intruded mercury volumen showed the pore diameter of 74.3–1.351 µm for $C_2S(2P_6)C_2S$ 3D scaffold and 86.13–1.46 µm for $C_2S(2P_6)C_2S$/Sr, respectively (Fig. 4A). The total porosity of 3D scaffolds showed insignificant pore sizes varying from 31.66 to 32.14% (small

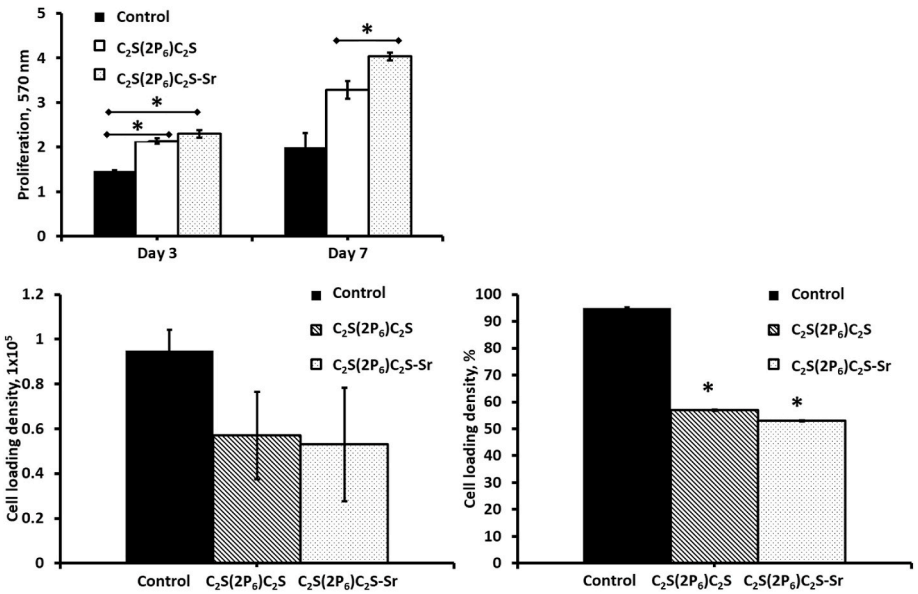

Fig. 5. Proliferation and cell loading density of MSCs on $C_2S(2P_6)C_2S$, $C_2S(2P_6)C_2S/Sr$ 3D scaffolds and control, respectively. * indicates the statistical significance, $P < 0.05$.

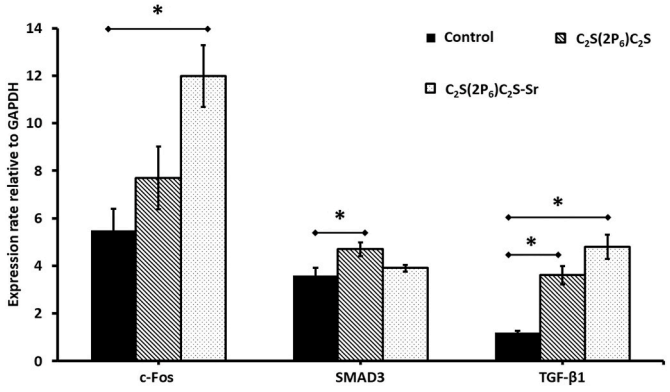

Fig. 6. mRNA Expression of proliferation genes by RT-qPCR of control, C2S (2P6)C2S and $C_2S(2P_6)C_2S/Sr$ 3D scaffolds, respectively. * indicates the statistical significance, $P < 0.05$. The expression of target genes was normalized with the housekeeping gene (GAPDH).

pores <300 μm) and ~78% (larger pores >300 μm) between $C_2S(2P_6)C_2S$ and $C_2S(2P_6)C_2S/Sr$ 3D scaffolds, respectively. The 3D scaffolds had four porous diameter peaks of 106, 12.20, 4.60 and 3.30 μm for $C_2S(2P_6)C_2S$ 3D scaffold, and 106.40, 16.74, 12.18 and 12.20 μm for $C_2S(2P_6)C_2S/Sr$ 3D scaffolds (Fig. 4B). However, the specific surface area of $C_2S(2P_6)C_2S/Sr$ 3D scaffolds (0.347 m^2/g) decreased compared to the specific surface area of $C_2S(2P_6)C_2S$ 3D scaffolds (1.417 m^2/g). All the above findings proved that the physical characteristics of ceramic/glass/ceramic 3D scaffolds did not drastically influence by strontium.

The proliferation rate of MSCs was increased significantly by both $C_2S(2P_6)C_2S$ and $C_2S(2P_6)C_2S/Sr$ 3D scaffolds compared to the control group irrespective of the culture time (Fig. 5A). In the control group, the cell proliferation rate of 7-days culture was increased compared to 3-days culture. On day 3, there was no significant difference in proliferation observed between $C_2S(2P_6)C_2S$ and $C_2S(2P_6)C_2S/Sr$ 3D scaffolds cultured cells, however, $C_2S(2P_6)C_2S/Sr$ 3D scaffold cultured cells showed more proliferative rate compared to $C_2S(2P_6)C_2S$ 3D scaffold on day 7 ($P < 0.05$). Among all groups, the $C_2S(2P_6)C_2S$ and $C_2S(2P_6)C_2S/Sr$ 3D scaffolds cultured cells showed a better proliferation rate on day 7 culture.

In general, the 3D scaffolds had lower cell loading ability compared to the control group (Fig. 5B and C). However, there was no significant difference in the cell loading density between $C_2S(2P_6)C_2S$ and $C_2S(2P_6)C_2S/Sr$ 3D scaffold groups. The total percentage of cells attached in control group was about 95%, which was decreased significantly in 3D scaffold groups (53–57%).

The proliferative mRNA expression of MSCs was assessed through three different genes such as c-Fos, SMAD3 and TGF-β1 (Fig. 6). In the control group, c-Fos mRNA was expressed more after 7-days culture, followed by SMAD3 and TGF-b1. Interestingly, the expression of c-Fos was increased in cells cultured on $C_2S(2P_6)C_2S/Sr$ 3D scaffold compared to cells cultured on $C_2S(2P_6)$C2S 3D scaffold and control group ($P < 0.05$), however, the cells proliferated in $C_2S(2P_6)$C2S 3D scaffold did not show any significant changes in c-Fos mRNA expression compared to the control group. On the contrary, the expression of SMAD3 was significantly increased in cells cultured on $C_2S(2P_6)C_2S$ 3D scaffold compared to cells cultured on $C_2S(2P_6)C_2S/Sr$ 3D scaffold and control groups. However, no significant changes were observed in SMAD3 mRNA expression between $C_2S(2P_6)C_2S/Sr$ 3D scaffold and control groups. Similar to c-Fos, the mRNA expression of TGF-β1 was significantly higher in cells cultured on $C_2S(2P_6)C_2S$ and $C_2S(2P_6)C_2S/Sr$ 3D scaffolds groups compared to the control cells ($P < 0.05$). Among the 3D scaffolds groups, the TGF-β1 mRNA expression was upregulated more in cells cultured on $C_2S(2P_6)C_2S/Sr$ 3D scaffold compared to cells cultured on $C_2S(2P_6)C_2S$ group.

The osteogenic stimulatory effect of 3D scaffolds was evidenced by the mineral staining of cells cultured with and without osteogenic medium for 21 days. As evidenced in Fig. 7, the control cells cultured in mesenchymal stem cell culture medium had no positive stains by alizarin red and von kossa dyes (Fig. 7 A and B). Surprisingly, the cells cultured on 3D scaffolds in mesenchymal stem cell culture medium were slightly stained for alizarin red and von kossa dyes. More specifically, the cells cultured on $C_2S(2P_6)C_2S/Sr$ 3D scaffold without osteogenic medium showed a higher level of positive staining for von kossan stain compared to cells cultured on $C_2S(2P_6)$C2S 3D scaffold. As expected, the control cells cultured with osteogenic differentiation medium showed positive staining for both alizarin red and von kossa dyes, which was not observed in control cells cultured without osteogenic medium. The mineral staining rate of differentiated MSCs was significantly upregulated in 3D scaffolds compared to control cells, with higher mineral staining in cells cultured on $C_2S(2P_6)C_2S/Sr$ 3D scaffold. Similar to

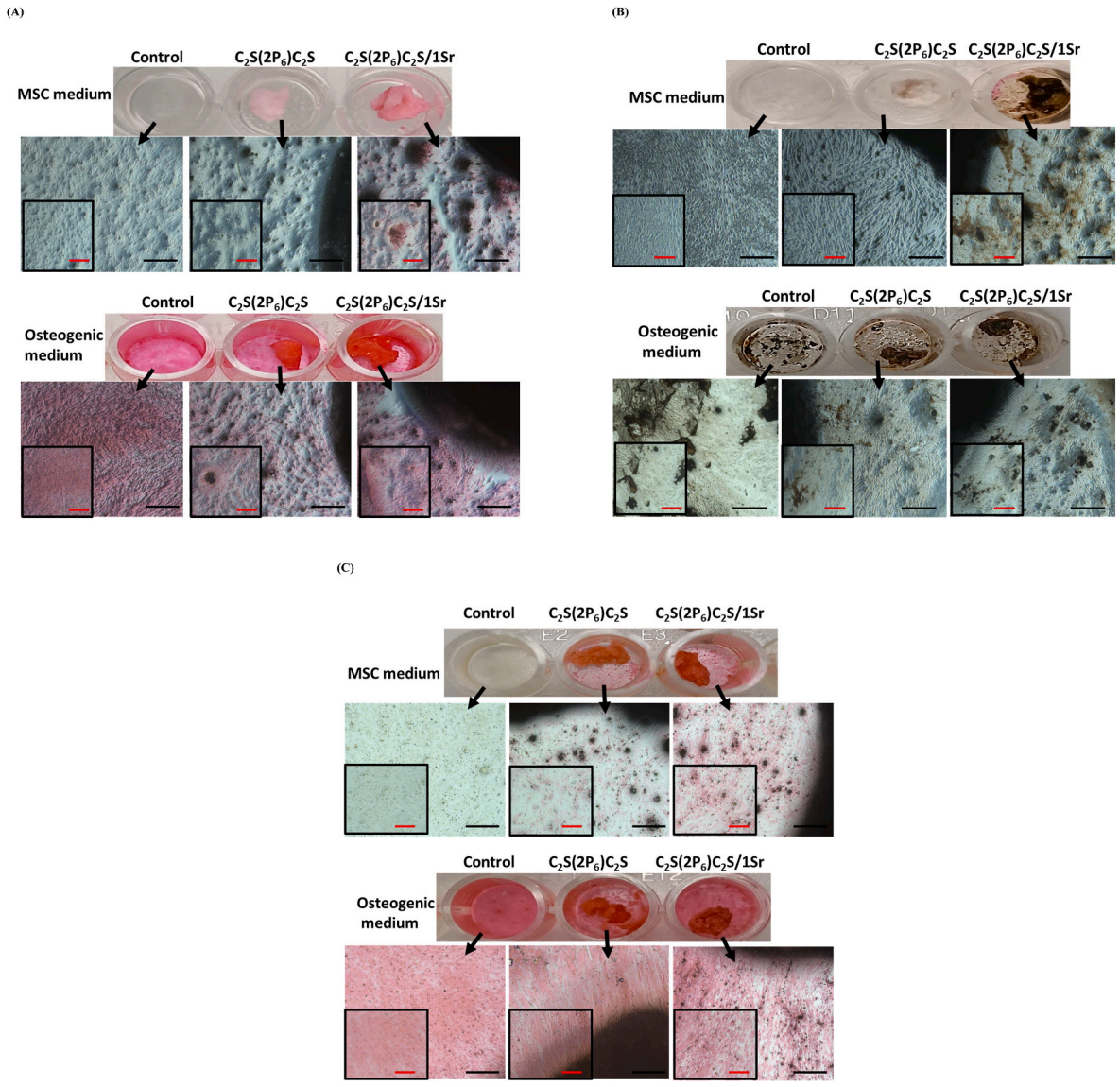

Fig. 7. Alizarin Red (A), Von Kossa (B) and ALP (C) staining of differentiated MSC cells. Control-cells without 3D scaffolds. C2S(2P6)C2S and $C_2S(2P_6)C_2S/Sr$ represent the MSCs differentiated on C2S(2P6)C2S and $C_2S(2P_6)C_2S/Sr$ 3D scaffolds, respectively. Scale bars- 200 μm (50 μm-insert). (For interpretation of the references to colour in this figure legend, the reader is referred to the Web version of this article.)

mineral staining, there was no positive staining for ALP stain in control cells cultured in mesenchymal stem cell culture medium, however, the cells stained positively when cultured on $C_2S(2P_6)C_2S/Sr$ 3D scaffold (Fig. 7C). As expected, the control cells cultured with osteogenic differentiation medium showed positive staining for ALP stain and the level of ALP staining was increased in cells cultured on 3D scaffolds, especially in $C_2S(2P_6)C_2S/Sr$ 3D scaffold.

The osteogenic potential of 3D scaffolds at the molecular level was evaluated by the qRT-PCR method using different osteogenic mRNA markers such as collagen type I, Runx2, ALP and osteocalcin (Fig. 8). During the investigation, the cells were cultured in two different culture mediums such as mesenchymal stem cell medium for control and osteogenic stimulatory supplement medium for the osteogenic group. The cells cultured in mesenchymal stem cell medium for 21 days did not upregulate the collagen type I mRNA expression in all the groups including control and 3D scaffolds groups. However, the mRNA expression of collagen type I level was significantly increased in control cells cultured with osteogenic culture medium for 21 days compared to the mesenchymal stem cell culture medium cultured control cells. Among the osteogenic supplemented groups, the level of collagen type I mRNA expression was increased in cells cultured on 3D scaffolds compared to control. The level of upregulation was more pronounced in cells cultured on $C_2S(2P_6)C_2S/Sr$ 3D scaffold than in cells cultured on $C_2S(2P_6)$C2S 3D scaffold ($P < 0.05$).

Surprisingly, the mRNA expression of the transcription factor, Runx2 which is primarily responsible for osteogenic differentiation, was significantly upregulated in cells cultured with mesenchymal stem cell medium on $C_2S(2P_6)C_2S/Sr$ 3D scaffold, but, it was not upregulated in the control cells and $C_2S(2P_6)C_2S$ 3D scaffold cultured cells. On the other side, the control cells cultured with osteogenic-supplemented culture medium expressed Runx2 mRNA, which was upregulated by culturing the cells on 3D scaffolds. More specifically, the level of Runx2 mRNA expression was upregulated in cells cultured on $C_2S(2P_6)C_2S/Sr$ 3D scaffold ($P < 0.05$) than in cells cultured on $C_2S(2P_6)C_2S$ 3D scaffold. Amongthe mesenchymal and osteogenic culture medium cultured cells, the Runx2 mRNA expression was highly upregulated in cells cultured on $C_2S(2P_6)C_2S/Sr$ 3D scaffold in osteogenic culture medium.

The level of ALP, an early osteogenic marker, was not detected in the control cells cultured in mesenchymal stem cell culture medium, however, the cells cultured on $C_2S(2P_6)C_2S/Sr$ 3D scaffolds slightly

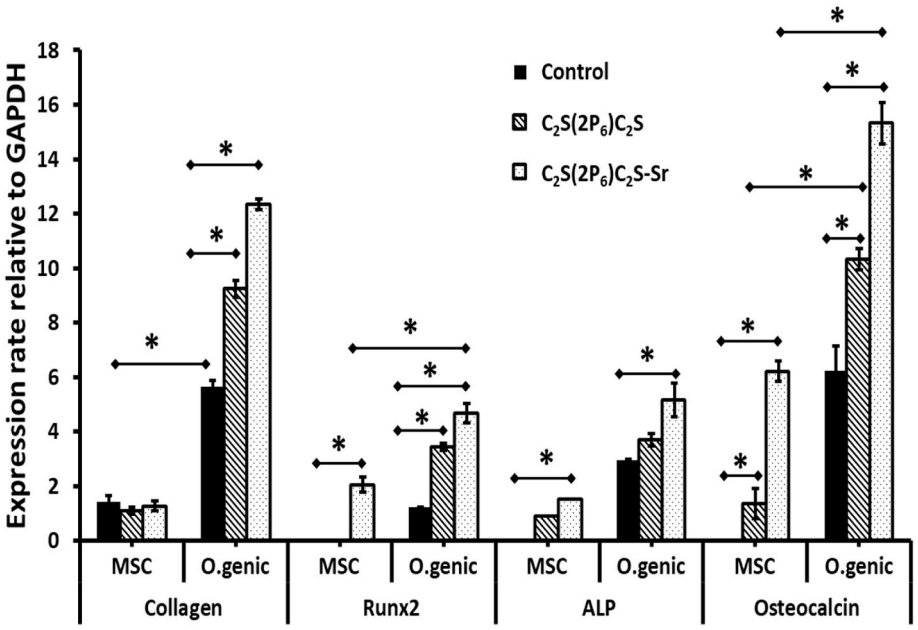

Fig. 8. Osteogenic genes expression of differentiated MSCs by RT-qPCR. Control-cells without 3D scaffolds. C2S(2P6)C2S and $C_2S(2P_6)C_2S$/Sr represent the MSCs cultured on C2S(2P6)C2S and $C_2S(2P_6)C_2S$/Sr 3D scaffolds, respectively. * indicates the statistical significance, $P < 0.05$. The expression of target genes was normalized with the housekeeping gene (GAPDH).

expressed ALP level, which was similar to the ALP histological staining results (Fig. 7). In contrast, the control cells expressed ALP mRNA to some extent when cultured with osteogenic supplement medium and the level of expression was significantly upregulated ($P < 0.05$) in cells cultured on $C_2S(2P_6)C_2S$/Sr 3D scaffold group. However, no significant difference in ALP mRNA level was observed between control and $C_2S(2P_6)C_2S$ 3D scaffold.

Similar to Runx2, the cells cultured with mesenchymal stem cell culture medium expressed osteocalcin mRNA except for the control group. In other words, the 3D scaffolds triggered the osteogenic differentiation of MSCs even without any osteogenic supplements. Interestingly, the induction level of osteocalcin mRNA expression without osteogenic supplement was significantly increased in cells cultured on $C_2S(2P_6)C_2S$/Sr 3D scaffold compared to $C_2S(2P_6)$C2S 3D scaffold. As expected, the control cells cultured with osteogenic medium expressed higher osteocalcin mRNA and the stimulatory effect of osteocalcin mRNA expression was increased by 3D scaffolds. Among the 3D scaffolds cultured cells, $C_2S(2P_6)C_2S$/Sr 3D scaffold upregualted more osteocalcin mRNA expression than $C_2S(2P_6)$C2S 3D scaffold ($P < 0.05$). Compared to mesenchymal culture medium, the level of osteocalcin mRNA expression was more upregulated in 3D scaffolds cultured cells with osteogenic supplement medium, especially in $C_2S(2P_6)C_2S$/Sr 3D scaffold cultured cells.

The morphological characteristic features and cell adhesion behavior of MSCs with 3D scaffolds were evaluated by scanning electron microscopy and fluorescence staining method using FITC and DAPI (Figs. 9 and 10). The control cells cultured for 7 days showed dense fiber structure and were arranged as clusters regardless of culture mediums such as mesenchymal and osteogenic differentiation mediums. The morphological images revealed that the cells completely covered the whole surface of the 3D scaffolds and were firmly adhered to the porous scaffolds. Interestingly, the cells cultured on 3D scaffolds showed unique morphology similar to biological tissues, especially $C_2S(2P_6)C_2S$/Sr 3D scaffold cultured cells. At the same time, the cells cultured on $C_2S(2P_6)C_2S$ 3D scaffolds were more globular in size, whereas, more flattened interconnected 3D structures were observed in $C_2S(2P_6)C_2S$/Sr 3D scaffold cultured cells (Fig. 10). The microstructural images of differentiated MSCs were shown in Fig. 11. As evidenced by the mineral staining and mRNA expression, $C_2S(2P_6)C_2S$/Sr 3D scaffold could initiate osteogenic differentiation of MSCs i.e. the cells cultured on $C_2S(2P_6)C_2S$/Sr 3D scaffold with MSC culture medium showed similar morphological features of those cells cultured on $C_2S(2P_6)C_2S$/Sr 3D scaffold with osteogenic culture medium (Fig. 11). However, the cells cultured on $C_2S(2P_6)$C2S 3D scaffold with MSC culture medium showed more flattened and dense morphology, which was significantly altered by culturing the cells in osteogenic culture medium (more fibrillar, thin and interconnected mesh network). Interestingly, the morphology was not significantly transformed between cells cultured with MSCs culture medium and osteogenic culture medium. All the above findings revealed that the $C_2S(2P_6)C_2S$/Sr 3D scaffold alone could promote osteogenic differentiation of MSCs without any additional osteogenic supplements.

4. Discussion

In the present study, for the first time, calcium silicate-calcium pyrophosphate-based 3D scaffolds, comprising a C_2S core, middle layer of $2P_6$ and the outer layer of C_2S, were fabricated by sol-gel method and the 3D scaffold's surface was coated with strontium to enhance the biological properties of the 3D scaffolds. To obtain a coherent and non-disintegrating three-layer material, the different layers of the scaffold were fabricated. According to the $CaO–P_2O_5$ phase diagram [39], $Ca_2P_6O_{17}$ showed a first appearance of a liquid phase below ~800 °C. This glass reacted with the surrounding C_2S phase transforming the nominal ceramic/glass/ceramic composition ($Ca_2SiO_4/Ca_2P_6O_{17}/Ca_2SiO_4$) into a material of composition $Ca_2P_2O_7$, $CaSiO_3$ and SiO_2 (Fig. 2). The glass phase did not disintegrate due to the interaction of the glass phase to the different crystalline phases of the scaffold. The porosity of scaffolds did not vary much between scaffolds with average porosity of <300 μm (31.66% and 32.14%) for $C_2S(2P_6)C_2S$ and $C_2S(2P_6)C_2S$/Sr 3D scaffolds, respectively. The porosity of 3D scaffolds proved the suitability for cell development, orientation and directionality of cell growth [40]. The presence of macropores (about 100–300 μm measured by the mercury porosimetry method and Archimedes's principles) could improve the nutrient supply and removal of cell debris for the regeneration of mineralized bone [41]. Importantly, the Sr coating did not influence the surface morphology (Fig. 1) and porosity (Fig. 4) of 3D

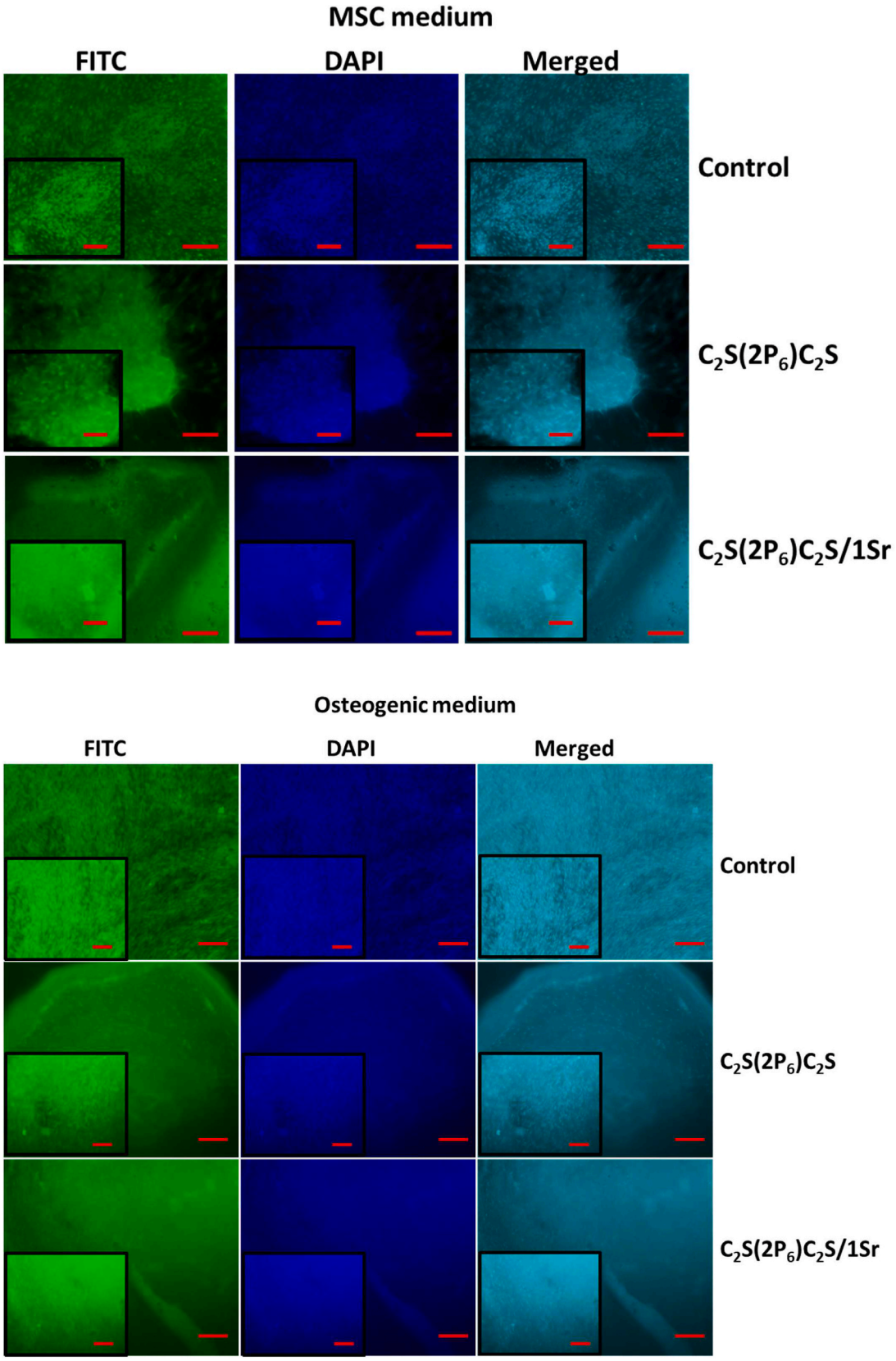

Fig. 9. Fluorescence staining of differentiated MSC cells with and without osteogenic culture medium. Control, $C_2S(2P_6)C_2S$ and $C_2S(2P_6)C_2S$/Sr represent the MSCs cultured on without 3D scaffolds, C2S(2P6)C2S and $C_2S(2P_6)C_2S$/Sr 3D scaffolds, respectively. FITC and DAPI stains confirmed the adherence of cells firmly on 3D scaffolds regardless of the culture medium. Images were captured at 4 × and 10 × magnification (insert). Scale bar: 200 μm and 100 μm (insert).

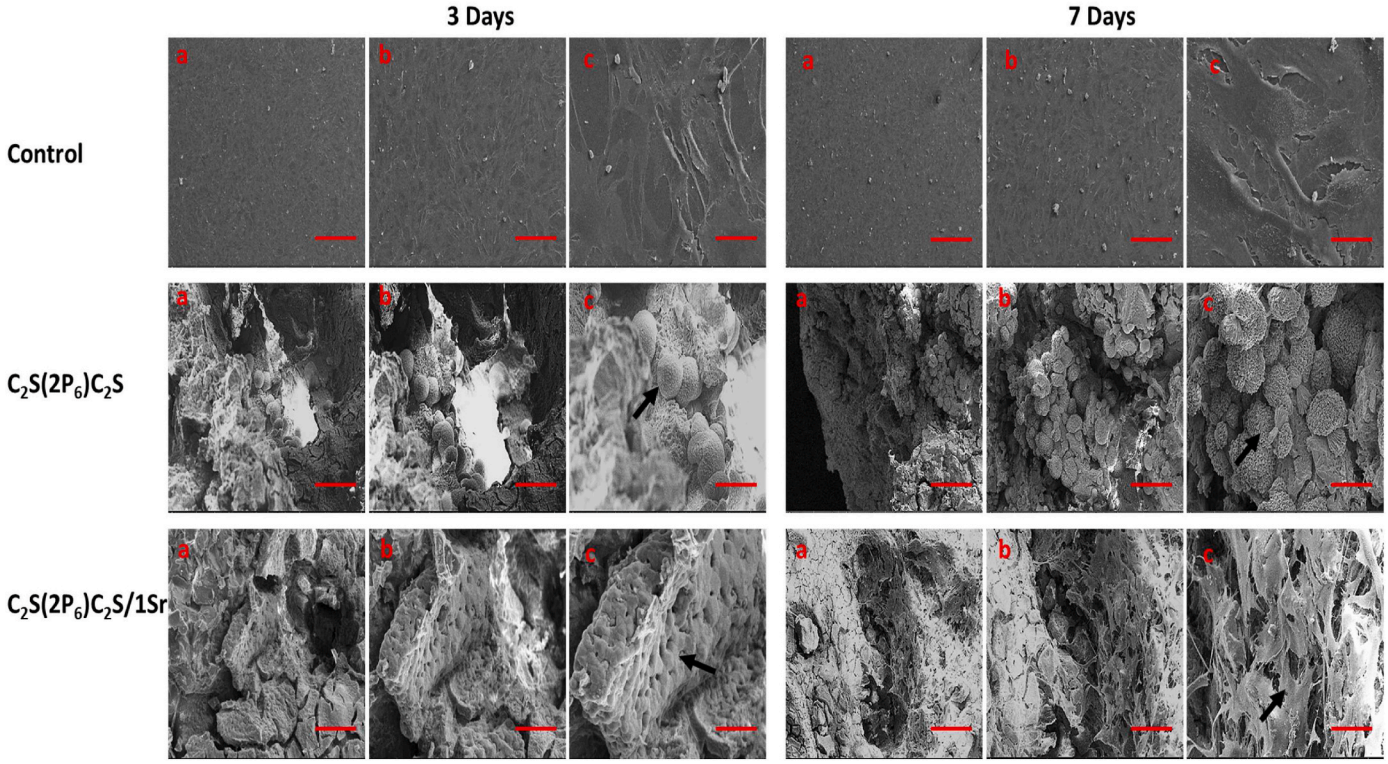

Fig. 10. Microstructural analysis of MSCs cultured with 3D scaffolds by SEM microscopy. The cells were cultured for 3 days and 7 days. Control- MSC cells cultured on glass. $C_2S(2P_6)C_2S$ and $C_2S(2P_6)C_2S$/Sr- MSCs cultured on $C_2S(2P_6)C_2S$ and $C_2S(2P_6)C_2S$/Sr 3D scaffolds. Black arrow shows the cells adhered on scaffolds. Alphabets a,b and c were different magnification with 400 μm, 200 μm and 50 μm scale bar, respectively.

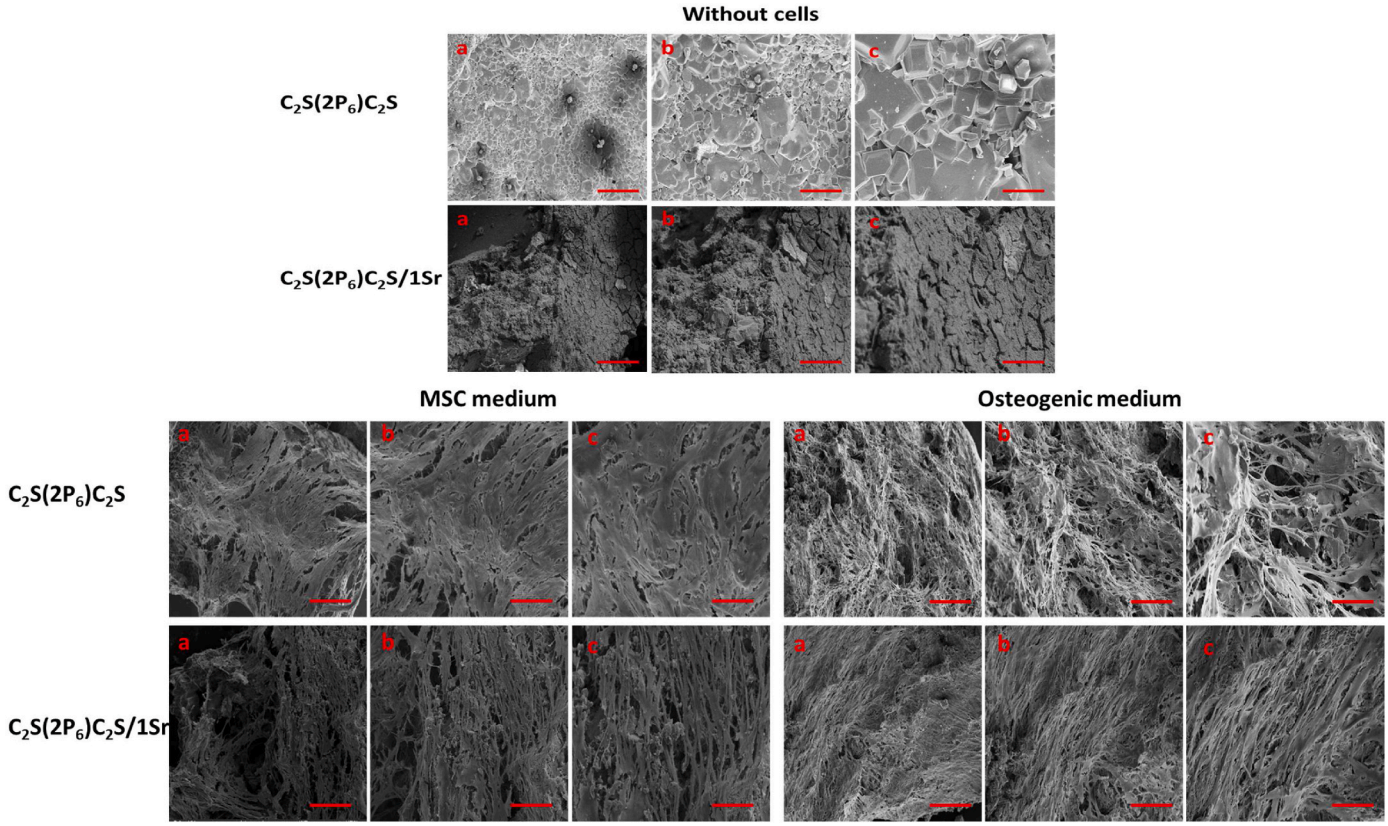

Fig. 11. SEM microscopic structure of differentiated MSCs cultured with 3D scaffolds. The cells were cultured for 21 days with MSC culture medium and osteogenic culture medium. A) Control scaffolds (without MSCs) and B) Differentitated MSCs on 3D scaffolds with culture medium. Alphabets a, b and c we different magnification with 400 μm, 200 μm and 50 μm scale bar, respectively.

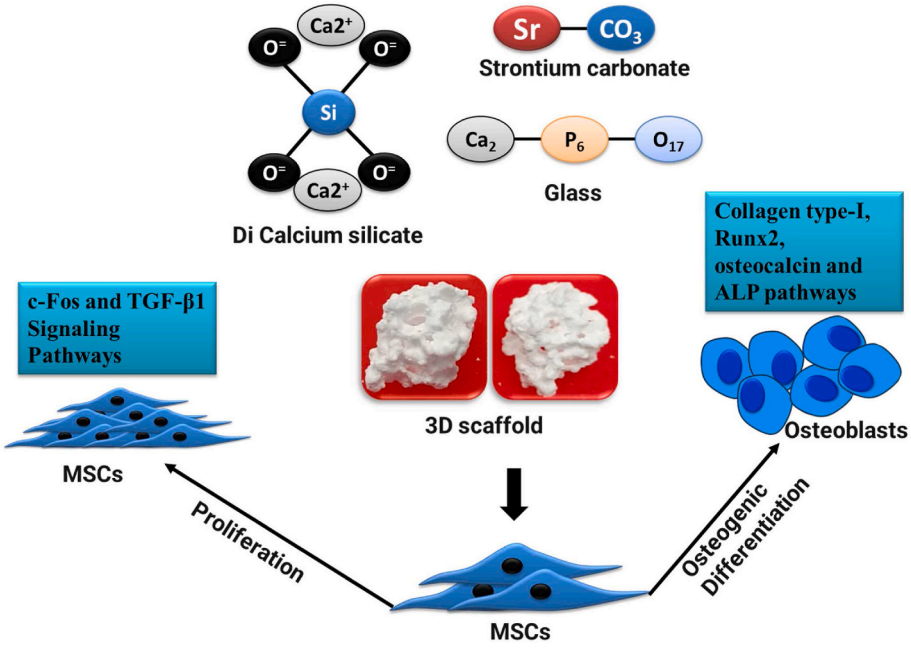

Fig. 12. The overall mechanism of $C_2S(2P_6)C_2S$/Sr 3D scaffolds in proliferation and osteogenesis behaviour of MSCs.

scaffold.

Both scaffolds showed a polyhedral grain structure, which was uniformly distributed throughout the matrix. Previously, Liu et al. reported the presence of homogenously distributed larger agglomerations of about 1~4 μm in Sr-coated C_2S powder and claimed that the surface morphology of C_2S did not alter by Sr coating [42], which supports the present study findings.

Compared to the control, the 3D scaffolds hold lesser cells in their internal structure, which might be due to their higher porous structure that allows cells easily pass through to the culture plate's bottoms after cell seeding. From the proliferation results, it is clear that 3D scaffolds could enhance the proliferation of MSCs, which proved the efficiency of 3D scaffolds in culturing stem cells for tissue regeneration applications. Interestingly, coating Sr could add more beneficial effects on cell proliferation in the present study. To support the present study, the proliferative ability of C_2S and Sr–C_2S cement using human bone marrow MSCs was investigated previously and reported that the proliferation rate of MSCs was significantly increased in cells treated with 25 to 3.125 mg mL^{-1} for C_2S bone cement and 3.125–100 mg mL^{-1} for Sr–C_2S bone cement compared to control [42]. Huang et al. also studied the proliferative effect of strontium-loaded bioactive calcium silicate bone cement. Similarly, Fada et al. evidenced the biocompatibility and non-toxicity of strontium nitrate coated dicalcium phosphate cement nanoparticles [43]. In another studies, human adipose derived MSCs cultured on PCL, PLLA and PVDF nanofibrous scaffolds, and hBMSCs seeded on layered double hydroxide (LDH)/polycaprolactone (PCL) nanocomposites showed higher proliferative rate on day 5 compared to respective controls, respectively [44,45].

The higher proliferative effect of cells cultured on $C_2S(2P_6)C_2S$/Sr 3D scaffold could be substantially evidenced by the higher mRNA expression of proliferative genes. More specifically, the proliferation of MSCs by $C_2S(2P_6)C_2S$/Sr 3D scaffold could enhance by increasing the expression of c-Fos and TGF-β1 proliferative genes. To support the present result, Yu et al. reported that the proliferation rate of osteoblastic MC3T3-E1 cells cultured on zinc-loaded calcium silicate-based ceramic was accelerated by increasing the TGF-β1 proliferative genes [46]. Another study reporting (Biodentine) tricalcium and dicalcium silicate (3CaO–SiO_2 and 2CaOSiO_2) concluded that the angiogenesis of dental pulp stem cells was induced by upregulating TGF-β1 and vascular endothelial growth factor (VEGF) mRNA expression [47]. Several studies reported the proliferative effect of C_2S in MSCs and osteogenic differentiation of MSCs [48–51].

The results of mineral staining and mRNA expression of osteogenic genes highlighted the osteogenic potential of 3D scaffolds, especially, the cells cultured on $C_2S(2P_6)C_2S$/Sr 3D scaffold could potentially differentiate into osteogenic cells even without osteogenic supplements. Interestingly, the $C_2S(2P_6)C_2S$/Sr 3D scaffolds alone stimulated the osteogenesis of MSCs cultured with mesenchymal stem cell culture medium. At the same time, $C_2S(2P_6)C_2S$ 3D scaffold also triggered osteogenic differentiation of MSCs without any supplements, but only to some lower extent and not enough to achieve complete osteogenic differentiation. To support the present study results, previous studies were investigated the osteogenic ability of biodentine (tricalcium and dicalcium silicate (3CaO SiO_2 and 2CaO SiO_2)) using dental pulp stem cells through alkaline phosphatase, osteopontin and sialophosphoprotein mRNA expression [47], zinc-loaded Ca–Si-based ceramic coating ($Ca_2ZnSi_2O_7$ coating and $CaSiO_3$ coating) using osteoblastic MC3T3-E1 cells through alkaline phosphatase, procollagen α_1(I), osteocalcin) and insulin-like growth factor-I (IGF-I) mRNA expression [46], Sr-loaded-bioactive calcium silicate bone cement using human mesenchymal stem cells through ALP and osteocalcin [52], Sr nitrate loaded dicalcium phosphate (DCaP) bone cement using human gingival fibroblasts (HuGu) cells through ALP [43], and Sr-loaded dicalcium silicate bone cement using hBMSCs through ALP [42]. Similar to the gene expression of present study, Abazari et al. reported that the differentiation of human adipose derived MSCs on PCL, PLLA and PVDF nanofibrous scaffolds expressed higher osteogenic gene expression of Runx-2, osteonectin, collagen-I and osteocalcin than control [44]. Also, Enderami et al. reported higher levels of ALP and Runx2 gene expression in hBMSCs differentiated on PCL/LDH nanocomposites [45]. The SEM morphology claimed that the $C_2S(2P_6)C_2S$/Sr 3D scaffold triggered the osteogenic differentiation of MSCs even without osteogenic supplements. This result further evidenced the earlier findings of mineral staining and mRNA expression of MSCs, which substantially proved the osteogenic stimulatory response of $C_2S(2P_6)C_2S$/Sr 3D scaffold. The present study accordingly disclosed that the $C_2S(2P_6)C_2S$/Sr 3D scaffold upregulated the proliferation of MSCs through c-Fos/TGF-β1 signaling pathways, and triggered osteogenic differentiation of MSCs through collagen type-I, Runx2, osteocalcin and ALP pathways (Fig. 12).

5. Conclusion

In the present study, the ceramic/glass/ceramic 3D scaffolds of nominal composition ($Ca_2SiO_4/Ca_2P_6O_{17}/Ca_2SiO_4$) were successfully fabricated by the sol-gel method together with the polymeric replica technique and coated with strontium. Characterization of scaffolds revealed that the coating of strontium did not affect the porosity and pore size of scaffolds, and XRD data confirmed the presence of calcium diphosphate, tridymite and calcium silicate. The ceramic/glass/ceramic 3D scaffolds upregulated the proliferation rate and proliferative genes (c-Fos and TGF-β1) of MSCs, especially by $C_2S(2P_6)C_2S$/Sr 3D scaffold. The cells cultured in mesenchymal stem cells did not differentiate into osteogenic cells unless treated with $C_2S(2P_6)C_2S$/Sr 3D scaffold. Interestingly, the $C_2S(2P_6)C_2S$/Sr 3D scaffold alone stimulated the osteogenic differentiation of MSCs without any osteogenic supplement and the osteogenic stimulatory effect of the $C_2S(2P_6)C_2S$/Sr 3D scaffold was more pronounced with osteogenic supplement medium. Overall, the study concluded that the fabricated strontium coated-3D scaffold ($C_2S(2P_6)C_2S$/Sr) could stimulate osteogenic differentiation of stem cells without any supplement and therefore could have great potential in bone and dental tissue regeneration. However, in the present study, the major limitations are the lack of information on the molecular signaling mechanism of fabricated 3D scaffolds in bone regeneration and the supported in-vivo evidence, which need to be explored in future research.

Funding

This work was financially supported by the projects PID2020-116693RB-C21 and PID2020-116693RB-C22, funded by MCIN/AEI/10.13039/501100011033 Spain and also the grant CIAICO/2021/157 funded by Generalitat Valenciana Spain.

CRediT authorship contribution statement

Jeevithan Elango: Conceptualization, Methodology, Data curation, Visualization, Investigation, Writing – original draft, Writing - review. Karina Salazar: Fabrication of 3D scaffold, characterization, Writing - review. Pablo Velasquez: Fabrication of 3D scaffold, Writing – review. Angel Murciano: Fabrication of 3D scaffold, characterization. Piedad N. de Aza: Fabrication and characterization of 3D scaffold, funding acquisition, project administration, writing- original draft and review. Wenhui Wu: Investigation and review. José Manuel Granero Marín: Data interpretation, Writing-review. Jose E. Mate Sanchez de Val: Funding acquisition, project administration, Writing-original draft.

Declaration of competing interest

The authors declare that they have no known competing financial interests or personal relationships that could have appeared to influence the work reported in this paper.

References

[1] J. Henkel, M.A. Woodruff, D.R. Epari, R. Steck, V. Glatt, I.C. Dickinson, P. F. Choong, M.A. Schuetz, D.W. Hutmacher, Bone regeneration based on tissue engineering conceptions—a 21st century perspective, Bone research 1 (1) (2013) 216–248.
[2] N. Ashammakhi, M.A. Darabi, N.S. Kehr, A. Erdem, S.-k. Hu, M.R. Dokmeci, A. S. Nasr, A. Khademhosseini, Advances in controlled oxygen generating biomaterials for tissue engineering and regenerative therapy, Biomacromolecules 21 (1) (2019) 56–72.
[3] L. Chen, L. Cheng, Z. Wang, J. Zhang, X. Mao, Z. Liu, Y. Zhang, W. Cui, X. Sun, Conditioned medium-electrospun fiber biomaterials for skin regeneration, Bioact. Mater. 6 (2) (2021) 361–374.
[4] A. Bharadwaz, A.C. Jayasuriya, Recent trends in the application of widely used natural and synthetic polymer nanocomposites in bone tissue regeneration, Mater. Sci. Eng. C 110 (2020) 110698.
[5] S. Ullah, X. Chen, Fabrication, applications and challenges of natural biomaterials in tissue engineering, Appl. Mater. Today 20 (2020) 100656.
[6] A. Kamatar, G. Gunay, H. Acar, Natural and synthetic biomaterials for engineering multicellular tumor spheroids, Polymers 12 (11) (2020) 2506.
[7] H. Gul, M. Khan, A.S. Khan, Bioceramics: Types and Clinical Applications, Handbook of Ionic Substituted Hydroxyapatites, Elsevier, 2020, pp. 53–83.
[8] M. Nabiyouni, T. Brückner, H. Zhou, U. Gbureck, S.B. Bhaduri, Magnesium-based bioceramics in orthopedic applications, Acta Biomater. 66 (2018) 23–43.
[9] R. Kumar, S. Mohanty, Hydroxyapatite: a versatile bioceramic for tissue engineering application, J. Inorg. Organomet. Polym. Mater. (2022) 1–17.
[10] H. Jodati, B. Yılmaz, Z. Evis, A review of bioceramic porous scaffolds for hard tissue applications: effects of structural features, Ceram. Int. 46 (10) (2020) 15725–15739.
[11] A. Namdar, E. Salahinejad, Advances in ion-doping of Ca-Mg silicate bioceramics for bone tissue engineering, Coord. Chem. Rev. 478 (2023) 215001.
[12] W. Hong, Q. Zhang, H. Jin, L. Song, Y. Tan, L. Luo, F. Guo, X. Zhao, P. Xiao, Roles of strontium and hierarchy structure on the in vitro biological response and drug release mechanism of the strontium-substituted bioactive glass microspheres, Mater. Sci. Eng. C 107 (2020) 110336.
[13] J.E.M.-S. de Val, J.L. Calvo-Guirado, J.M.G. Marín, G.G. Moreno, P. Mazón, P.N. de Aza, Material characterization and in vivo behavior of dicalcium silicate cement modified with phosphorus, Ceram. Int. 42 (1) (2016) 952–960.
[14] F. Zuleta, A. Murciano, S.A. Gehrke, J.E. Maté-Sánchez de Val, J.L. Calvo-Guirado, P.N. De Aza, A new biphasic dicalcium silicate bone cement implant, Materials 10 (7) (2017) 758.
[15] H. Agourrame, J. Moudar, N. Khachani, M. Taibi, A. Diouri, Mineralogical stabilization and morphology of hardystonite Petedunnite-Dicalcium silicate ternary mixtures, Mater. Today: Proc. 58 (2022) 1515–1519.
[16] M.G. Gandolfi, F. Zamparini, S. Valente, G. Parchi, G. Pasquinelli, P. Taddei, C. Prati, Green hydrogels composed of sodium mannuronate/guluronate, gelatin and biointeractive calcium silicates/dicalcium phosphate dihydrate designed for oral bone defects regeneration, Nanomaterials 11 (12) (2021) 3439.
[17] H. Li, J. Sun, Effects of dicalcium silicate coating ionic dissolution products on human mesenchymal stem-cell proliferation and osteogenic differentiation, J. Int. Med. Res. 39 (1) (2011) 112–128.
[18] W. Cheng, J. Chang, Fabrication and characterization of polysulfone-dicalcium silicate composite films, J. Biomater. Appl. 20 (4) (2006) 361–376.
[19] P. Mazón, N. Piedad, Porous scaffold prepared from α′ L-Dicalcium silicate doped with phosphorus for bone grafts, Ceram. Int. 44 (1) (2018) 537–545.
[20] C.M. Primus, F.R. Tay, L.-n. Niu, Bioactive tri/dicalcium silicate cements for treatment of pulpal and periapical tissues, Acta Biomater. 96 (2019) 35–54.
[21] C. Wu, J. Chang, A review of bioactive silicate ceramics, Biomed. Mater. 8 (3) (2013) 032001.
[22] D. Wang, J. Chang, Comparison on accelerated carbonation of β-C2S, Ca (OH) 2, and C4AF: reaction degree, multi-properties, and products, Construct. Build. Mater. 224 (2019) 336–347.
[23] L. Huang, L. Tang, H. Gu, Z. Li, Z. Yang, New insights into the reaction of tricalcium silicate (C3S) with solutions to the end of the induction period, Cement Concr. Res. 152 (2022) 106688.
[24] H. Fleisch, S. Bisaz, Mechanism of calcification: inhibitory role of pyrophosphate, Nature 195 (4844) (1962), 911-911.
[25] X. Yan, Q. Zhang, X. Ma, Y. Zhong, H. Tang, S. Mai, The mechanism of biomineralization: progress in mineralization from intracellular generation to extracellular deposition, Japanese Dental Science Review 59 (2023) 181–190.
[26] L. Fu, M. Pujari-Palmer, C. Öhman-Magi, H. Engqvist, W. Xia, Calcium phosphate cements: structure-related properties, The Chemistry of Inorganic Biomaterials 7 (2021) 99.
[27] L.M. Grover, A.J. Wright, U. Gbureck, A. Bolarinwa, J. Song, Y. Liu, D.F. Farrar, G. Howling, J. Rose, J.E. Barralet, The effect of amorphous pyrophosphate on calcium phosphate cement resorption and bone generation, Biomaterials 34 (28) (2013) 6631–6637.
[28] D. Stachel, H. Paulus, I. Svoboda, H. Fuess, Crystal structure of calcium ultraphosphate, Ca2P6O17, Z. Kristallogr. 202 (1–2) (1992) 117–118.
[29] M. Sahebalzamani, M. Ziminska, H.O. McCarthy, T.J. Levingstone, N.J. Dunne, A. R. Hamilton, Advancing bone tissue engineering one layer at a time: a layer-by-layer assembly approach to 3D bone scaffold materials, Biomater. Sci. 10 (11) (2022) 2734–2758.
[30] M. Teimoori, H. Nokhbatolfoghahaei, A. Khojasteh, Bilayer scaffolds/membranes for bone tissue engineering applications: a systematic review, Biomater. Adv. (2023) 213528.
[31] C. Bertsch, H. Maréchal, V. Gribova, B. Lévy, C. Debry, P. Lavalle, L. Fath, Biomimetic bilayered scaffolds for tissue engineering: from current design strategies to medical applications, Adv. Healthcare Mater. (2023) 2203115.
[32] Y. Li, Y. Liu, R. Li, H. Bai, Z. Zhu, L. Zhu, C. Zhu, Z. Che, H. Liu, J. Wang, Collagen-based biomaterials for bone tissue engineering, Mater. Des. 210 (2021) 110049.
[33] J. Reginster, Strontium ranelate in osteoporosis, Curr. Pharmaceut. Des. 8 (21) (2002) 1907–1916.
[34] Y. Zhang, X. Cui, S. Zhao, H. Wang, M.N. Rahaman, Z. Liu, W. Huang, C. Zhang, Evaluation of injectable strontium-containing borate bioactive glass cement with enhanced osteogenic capacity in a critical-sized rabbit femoral condyle defect model, ACS Appl. Mater. Interfaces 7 (4) (2015) 2393–2403.
[35] E. Bonnelye, A. Chabadel, F. Saltel, P. Jurdic, Dual effect of strontium ranelate: stimulation of osteoblast differentiation and inhibition of osteoclast formation and resorption in vitro, Bone 42 (1) (2008) 129–138.

[36] J. Elango, Proliferative and osteogenic supportive effect of VEGF-loaded collagen-chitosan hydrogel system in bone marrow derived mesenchymal stem cells, Pharmaceutics 15 (4) (2023) 1297.
[37] R. Wang, B. Bao, S. Wang, J. Elango, W. Wu, Fabrication of Chinese Traditional Medicines incorporated collagen biomaterials for human bone marrow mesenchymal stem cells, Biomed. Pharmacother. 139 (2021) 111659.
[38] J. Elango, K. Saravanakumar, S.U. Rahman, Y. Henrotin, J.M. Regenstein, W. Wu, B. Bao, Chitosan-collagen 3D matrix mimics trabecular bone and regulates RANKL-mediated paracrine cues of differentiated osteoblast and mesenchymal stem cells for bone marrow macrophage-derived osteoclastogenesis, Biomolecules 9 (5) (2019) 173.
[39] W.L. Hill, G.T. Faust, D.S. Reynolds, The binary system P 2 O 5; 2 CaO. P 2 O 5, Am. J. Sci. 242 (9) (1944) 457–477.
[40] K.A. Hing, Bioceramic bone graft substitutes: influence of porosity and chemistry, Int. J. Appl. Ceram. Technol. 2 (3) (2005) 184–199.
[41] V. Karageorgiou, D. Kaplan, Porosity of 3D biomaterial scaffolds and osteogenesis, Biomaterials 26 (27) (2005) 5474–5491.
[42] W. Liu, Z. Huan, M. Xing, T. Tian, W. Xia, C. Wu, Z. Zhou, J. Chang, Strontium-substituted dicalcium silicate bone cements with enhanced osteogenesis potential for orthopaedic applications, Materials 12 (14) (2019) 2276.
[43] R. Fada, M. Shahgholi, M. Karimian, Improving the mechanical properties of strontium nitrate doped dicalcium phosphate cement nanoparticles for bone repair application, Ceram. Int. 47 (10) (2021) 14151–14159.
[44] M.F. Abazari, Z. Hosseini, S.Z. Karizi, S. Norouzi, M. Amini Faskhoudi, E. Saburi, S. E. Enderami, A. Ardeshirylajimi, H. Mohajerani, Different osteogenic differentiation potential of mesenchymal stem cells on three different polymeric substrates, Gene 740 (2020) 144534.
[45] S.E. Enderami, S.S. Shafiei, M. Shamsara, S.E. Enderami, A.R. Tabari, Evaluation of osteogenic differentiation of bone marrow-derived mesenchymal stem cell on highly porous polycaprolactone scaffold reinforced with layered double hydroxides nanoclay, Front. Bioeng. Biotechnol. 10 (2022) 805969.
[46] J. Yu, K. Li, X. Zheng, D. He, X. Ye, M. Wang, In vitro and in vivo evaluation of zinc-modified Ca–Si-based ceramic coating for bone implants, PLoS One 8 (3) (2013) e57564.
[47] A.-R. Youssef, R. Emara, M.M. Taher, F.A. Al-Allaf, M. Almalki, M.A. Almasri, S. S. Siddiqui, Effects of mineral trioxide aggregate, calcium hydroxide, biodentine and Emdogain on osteogenesis, Odontogenesis, angiogenesis and cell viability of dental pulp stem cells, BMC Oral Health 19 (2019) 1–9.
[48] C.-C. Chen, C.-W. Wang, N.-S. Hsueh, S.-J. Ding, Improvement of in vitro physicochemical properties and osteogenic activity of calcium sulfate cement for bone repair by dicalcium silicate, J. Alloys Compd. 585 (2014) 25–31.
[49] J. Sun, J. Li, X. Liu, L. Wei, G. Wang, F. Meng, Proliferation and gene expression of osteoblasts cultured in DMEM containing the ionic products of dicalcium silicate coating, Biomed. Pharmacother. 63 (9) (2009) 650–657.
[50] M.G. Gandolfi, G. Ciapetti, P. Taddei, F. Perut, A. Tinti, M.V. Cardoso, B. Van Meerbeek, C. Prati, Apatite formation on bioactive calcium-silicate cements for dentistry affects surface topography and human marrow stromal cells proliferation, Dent. Mater. 26 (10) (2010) 974–992.
[51] W. Zhong, X. Li, J.L. Pathak, L. Chen, W. Cao, M. Zhu, Q. Luo, A. Wu, Y. Chen, L. Yi, Dicalcium silicate microparticles modulate the differential expression of circRNAs and mRNAs in BMSCs and promote osteogenesis via circ_1983–miR-6931–Gas7 interaction, Biomater. Sci. 8 (13) (2020) 3664–3677.
[52] T.-H. Huang, C.-T. Kao, Y.-F. Shen, Y.-T. Lin, Y.-T. Liu, S.-Y. Yen, C.-C. Ho, Substitutions of strontium in bioactive calcium silicate bone cements stimulate osteogenic differentiation in human mesenchymal stem cells, J. Mater. Sci. Mater. Med. 30 (2019) 1–13.